A Model of Pellet Ablation with a Multi-Species Ablatant

Forskningscenter Risø, Roskilde; Thomsen, K.; Piret, S.

Publication date:
1988

Document Version
Publisher's PDF, also known as Version of record

Risø-M-2748

RISØ

Risø-M-2748

A Model of Pellet Ablation with a Multi-Species Ablatant

C. T. Chang, K. Thomsen and S. Piret

Risø National Laboratory, DK-4000 Roskilde, Denmark
October 1988

Risø-M-2748

A MODEL OF PELLET ABLATION WITH A MULTI-SPECIES ABLATANT

C.T. Chang and K. Thomsen*
Risoe National Laboratory - Association Euratom

S. Piret
Laboratoire de Physique des Gaz et des Plasmas
Université Paris-sud, Orsay, France

Abstract. The single species neutral - shielding model for the ablation of a hydrogenic pellet is extended by considering the ablatant as a mixture of four species: molecular and atomic hydrogen, protons and electrons. Compared with the single-species - ablatant model, results of the analysis showed that the ablatant state differs considerably. The attenuation of the incoming electron energy and energy flux, however, are very much similar, irrespective of the ablatant composition. The scaling law of the pellet ablation rate with respect to the plasma state of T_e, n_e and the pellet radius, r_p remains the same; the ablation rate is reduced approximately by 15%. at some combinations of T_e, n_e and r_p, a weak shock can appear when the ablated flow downstream becomes sonic. A sufficient but not necessary condition for its occurence is that the ablatant approaches either a state of complete dissociation, or complete ionization. To study the possible existence of an effective energy absorbing spherical region around the pellet, a comparison between the local ablated electron collisional mean free path and the electron Larmor radius in the cloud is made. A critical field, B_c is then defined and evalued at the ionization radius, r_i. For plasma state of fusion interest and pellet radius beyond 0.15 mm, B_c is well above 10 Tesla.

* Present address; JET Joint Undertaking, Abingdon, Oxfordshire, UK.

October 1988

Risoe National Laboratory, DK-4000 Roskilde, Denmark

ISBN 87-550-1466-6
ISSN 0418-6435

Grafisk Service, Risø 1988

CONTENTS Page

1. INTRODUCTION

Present tokamak experiments showed that a longer global energy confinement time is often associated with a density profile which is centrally peaked. One possibility of achieving such a density profile is by high-speed pellet injection. [1]. As the required injection speed is closely related to the ablation rate of the pellet in the prevailing plasma environment, a detailed understanding of the ablation process, therefore, should be desirable.

Comparisons of current pellet injection experiments with theoretical predictions are based mainly on the "transonic neutral shielding" model (TNS) [2,3] and their modifications [4,5,6]. An essential feature of these models is that most of the energy of the incoming plasma electrons is absorbed in a thin spherical layer of the ablated cloud. Among many assumptions of these models, the ablatant is taken to be a single species, a neutral H_2 or D_2 gas. The expansion of the cloud is considered to be spherically symmetric near the pellet.

However, for a combination of plasma states, T_e, n_e and pellet radius, r_p of current interest, computational results showed that the equilibrium degree of dissociation, α_d at the sonic radius, r_*, is already appreciable, (e.g. at T_e = 600 eV, $n_e = 2 \times 10^{13}$ and r_p = 0.2 mm, α_d = 0.69). Although this estimated value of α_d is based on the original TNS model where the energy required for the dissociation process is neglected; nevertheless, one would expect that even with the correction, the presence of atomic hydrogen might not be negligible. When the ablatant expands further downstream, its pressure drops and its temperature rises through the interaction with the incoming hot plasma electrons. It is conceivable that for some combinations of plasma state and pellet radius that the degree of ionization of the ablatant could become sufficiently high to invalid the assumption of the spherical expansion. Such departures from the TNS model, in fact, have been observed experimentally. For example, holographic interferograms

of the ablated cloud taken in some of the ISX-B discharges indicated that the degree of ionization, α_i, already becomes noticeable ($\approx$ 2%) at an expansion radius less than 1.5 r_p [7]. Departures of the ablated cloud from spherical expansion also have been observed in image pictures of the cloud, [8], and the detections of striations [9,10] in several devices.

The modification of the TNS model by including the dissociation of the ablatant has been considered previously by Parks [11]. In his model, a constant ratio of the specific heats, γ was used, and the singularity of the momentum equation of the ablated fluid was taken at the sonic radius of the ablated cloud. It can be shown that for an arbitrary degree of dissociation, α_d, the singular point usually occurs within the sonic radius. Throughout this paper, sound speed refers to that of a local Frozen Flow. The singular point always occurs at the equilibrium sonic radius. In reality, Parks' treatment is limited to cases where complete dissociation occurs at the sonic radius.

Subsequently, Felber et al. treated the problem of dissociation and ionization of the ablatant more in detail [12]. They considered two cases: (a) surface dissociation and volume ionization, and (b) volume dissociation and ionization. In the first, the ablatant is assumed to leave the pellet surface as an atomic gas, and becomes subsequently ionized in the expanding cloud. At the pellet surface, they modified the boundary conditions of reference [2] by taking into account the finite energy required for dissociation, but retained the original assumption of vanishing surface temperature. In the second case of volume dissociation and ionization, they assumed that these two processes occur separtely, i.e. ionization hardly noticeable (< 1%) until dissociation is nearly completed (> 99%). The ratio of the specific heats was taken as a constant, $\gamma = 5/3$, throughout the expanding cloud.

As mentioned above, when dissociation and ionization effects are present, the singularity of the momentum equation, in general, does not occur at the sonic radius of the expanding cloud. Its

exact location depends on the freestream plasma state, T_e, n_e and the pellet radius, r_p; thus one has no a priori knowledge of its location. It is therefore doubtful that a reliable solution can be obtained by initiating the integration at the freestream as mentioned in reference [12]. For the same reason, although the separation of dissociation and ionization effects is a common practice in treating relaxation phenomena analytically, it could introduce an error in the starting slope at the singular point when the problem has to be treated numerically.

The attenuation of the incoming electron energy in the ablated cloud depends not only on the density distribution of the ablated material but also on its composition. It is not clear beforehand to what extent the ablation process occurring at the pellet surface could affect the state of the ablatant, the influence of the boundary condition at the pellet surface, therefore, remains to be examined. Furthermore, the analysis of [12] is limited to the ablation of a pellet in a homogeneous plasma of thermonuclear interest only.

When local thermodynamic equilibrium is invoked, the ablatant composition depends on the local pressure and temperature in the cloud, these parameters, in turn, are influenced strongly by the ambient plasma state and the pellet size. During the traverse of the pellet along its injected path in an experimental device, it is subjected to the variation of the plasma temperature and density prevailing in the device. A larger initial pellet is subjected to the lower temperature and density at the edge, whereas a smaller pellet near its end of travel is subjected to higher temperature and density in the core region of the device. In view of these facts and the assumptions as well as the limited treatment of reference [12] mentioned above, a reexamination of the subject matter and an extension of their analysis to cover a wide range of pellet size and plasma state of current interest, therefore, should be a worthwhile undertaking.

The paper is divided into four sections. After this introduction, the analytical model is formulated in Section 2; there the basic

assumptions, governing equations and boundary conditions as well as the method of solution are presented. In Section 3, the results of the analysis are given. Following a discussion about the effects of the specific heat ratio, γ, and of the ablation process at the pellet surface, the variation of the ablatant state in the cloud is shown explicitly. This is followed by a discussion of the ionization radius and the validity of the spherical expansion. Lastly, the possible occurrence of a second singularity (or a thermal shock) is analyzed. Finally the paper ends with a brief summary and discussion in Section 4.

2. ANALYTICAL MODEL

2.1. Basic assumptions

Similar to the TNS model, we shall consider the ablation of a spherical hydrogenic pellet subjected to the impact of a beam of monoenergetic electrons. The particle and energy flux of the beam is taken to be the same as that of a collection of plasma electrons having a Maxwellian energy distribution of n_e and T_e; thus the energy of the equivalent beam is given by $E = 2\ T_e$. The expansion of the ablated flow is assumed to be quasi-steady and spherical. The latter assumption implies that we expect the existence of a dense ablated layer surrounding the pellet where most of the energy of the incoming electrons is absorbed. In fact, the main objective of the paper is to investigate the relation of such a layer with respect to the ambient plasma state and pellet size.

The main departure of the present study from the TNS model is that instead of taking the ablatant to be a single species of molecular hydrogen (frozen flow), we assume it to be a mixture of four species, H_2, H, H^+ and e^-. Furthermore, we assume the existence of local thermodynamic equilibrium (LTE), so that the con-

centrations of these species are determined by the local temperature and pressure of the ablatant (equilibrium flow). No artificial separation of the dissociation and ionization region is therefore necessary.

A direct consequence of dissociation and ionization is the change of the average mass of the ablatant and its ratio of specific heats, γ. The average mass of the ablatant can be evaluated once the relative concentrations of the species are known. When the quantum mechanical effect is neglected, the variation of γ can be related to the corresponding variation of the degree of freedom; thus

$$\gamma = 1 + 2/f \ . \qquad (2)$$

If we assume f varies linearly with the degree of dissociation, α_d, then

$$\gamma = (7 - 2\ \alpha_d)/(5 - 2\ \alpha_d) \ . \qquad (2a)$$

Alternatively, since f varies only with the degree of dissociation, α_d, we take it as the average value of the mixture, H_2 and H, then

$$\gamma = (7 + 3\ \alpha_d)/(5 + \alpha_d), \ [12] \ . \qquad (2b)$$

2.2. Governing equations

The composition of the ablatant can be analyzed in terms of the degree of dissociation, α_d, and of ionization, α_i, defined respectively by

$$\alpha_d = n_H/(2\ n_{H_2} + n_H) \ , \qquad (3)$$

$$\alpha_i = n_{H^+}/(n_H + n_{H^+}) \ , \qquad (4)$$

where n_{H^+}, n_H and n_{H_2} are the particle densities of proton, and atomic and molecular hydrogen, respectively. Neglecting the elec-

tron mass compared to that of the proton, the concentration of the various species can be expressed in terms of α_d and α_i, thus

$$C_a = \frac{\rho_H}{\rho} = \frac{\alpha_d(1-\alpha_i)}{1-\alpha_i(1-\alpha_d)} \tag{5}$$

$$C_i = \frac{\rho_{H^+}}{\rho} = \frac{\alpha_d\alpha_i}{1-\alpha_i(1-\alpha_d)} \tag{6}$$

$$C_m = \frac{\rho_{H_2}}{\rho} = 1 - C_a - C_i \ . \tag{7}$$

In the above equations, ρ is the mass density of the mixture; ρ_{H_2}, ρ_H and ρ_{H^+} are the mass density of H_2, H and H^+ respectively.

Using Dalton's law of partial pressure and the LTE assumption, the total pressure of the ablatant can be written as

$$p = (1 + C_a + 3\ C_i)\ \rho T/2\ m_H \ .$$

Taking the mass of the mixture as given by

$$m = 2\ m_H/(1 + C_a + 3\ C_i) \ , \tag{8}$$

the equation of state then assumes the familiar form,

$$p = \rho T/m \ . \tag{9}$$

Invoking the law of mass action, the degree of dissociation and ionization can be written explicitly as

$$\left.\begin{aligned} \alpha_d &= \left[1 + \frac{p}{K_d(T)}\right]^{-1/2} , \\ K_d(T) &= 1.2401 \times 10^{12} T^{1.327} e^{(-E_d/T)} , \end{aligned}\right\} \tag{10}$$

$$\left.\begin{aligned} \alpha_i &= \left[1 + \frac{p}{K_i(T)}\right]^{-1/2} , \\ K_i(T) &= 4.8263 \times 10^9 T^{2.5} e^{(-E_i/T)} . \end{aligned}\right\} \qquad (11)$$

In the above equation, the dissociation and ionization energy, E_d and E_i, as well as the ablatant temperature, T, are in eV. The pressure p, and the equilibrium constants K_d, and K_i are in dynes/cm^2.

The dynamics of the expansion process is then described by the three conservation laws. Assuming the ablatant to be a nondissipative ideal gas and the expansion process to be spherical symmetry, the three conservation laws are given as

$$\frac{d}{dr}(\rho v r^2) = 0 , \qquad (12)$$

$$\rho v \frac{dv}{dr} + \frac{dp}{dr} = 0 , \qquad (13)$$

$$\rho v \frac{d}{dr}\left\{\xi \frac{T}{m} + \frac{v^2}{2} + \nu\right\} = Q(r) , \qquad (14)$$

where

$$\xi = \frac{\gamma}{\gamma - 1} , \qquad (15)$$

$$\nu = \frac{E_i}{m_H} C_i + \frac{E_d}{2m_H} C_a . \qquad (16)$$

Thus v is the specific energy of the fluid spent for the phase transition, and $Q(r)$ is the volumetric heat source. Following a similar argument of the TNS model, we take the attenuation of the energy flux of the incoming electrons in the ablatant as given by

$$\frac{dE}{dr} = \frac{\rho}{m_H} L(E) \tag{17}$$

$$\frac{dq}{dr} = \frac{\rho A(E)}{2m_H} q \tag{18}$$

where $A(E) \equiv 2\, L(E)/E + \sigma(E)$. (19)

For simplicity, we take the loss function, [3],

$$L(E) = [2.35 \times 10^{14} + 4 \times 10^{11}E + 2 \times 10^{17}E^{-2}]^{-1} \tag{20}$$

and the "effective scattering cross section", [2],

$$\sigma(E) = 1.13 \times 10^{-14}E^{-1} \qquad (E < 100 \text{ eV})$$

$$= 8.8 \times 10^{-13}E^{-1.71} - 1.62 \times 10^{-12}E^{-1.932} \qquad (E > 100 \text{ eV}) \tag{21}$$

to be the same as those corresponding to a stopping medium of molecular hydrogen gas. In these equations, E is in eV, $\sigma(E)$ in cm^2 and $L(E)$ in eV-cm^2. The derivations of Eqs. (17) and (18) and discussions concerning the validities of Eqs. (20) and (21) are given in the appendix. To complete the description, we shall take $Q(r)$ appearing in the energy conservation equation to be the same as the energy deposited per unit volume per second in the ablatant through the slowing down of the incoming electrons; thus

$$Q(r) = \frac{dq}{dr}. \tag{22}$$

2.3. Normalization

In the single species TNS model, the singularity of the system of equations governing the ablated flow occurs at the radius of expansion, r_*, where the flow becomes sonic, or the Mach number $M_* = 1$. Since M^2 can be expressed as the ratio of the kinetic to thermal energy of the flow, the occurrence of the singularity at $M_* = 1$ can be interpreted as an equipartition between the kinetic and thermal energies. When dissociation occurs, some energy must be spent for the phase transition. If the occurrence of the singularity of the governing equations depends on the distribution of the total energy of the flow among its various components, kinetic, thermal and potential, we may expect that when dissociation occurs, the singular radius, r_*, in general will be in the subsonic region.

Normalizing all the variables with respect to their corresponding values at r_*, e.g. $r = r_* r'$, $p = p_* p'$, etc., and introducing

$$\theta = T/T_* , \quad w = v^2/v_*^2 , \quad \mu = m_*/m , \quad \Lambda' = \Lambda(E)/\Lambda(E_*) , \qquad (23)$$

the system of equations can be written in their dimensionless form; thus after dropping the prime sign, they take the following expressions:

$$\rho\sqrt{w}\, r^2 = 1 \qquad (24)$$

$$\frac{dp}{dr} = - \frac{\gamma_* M_*^2}{2r^2\sqrt{w}} \frac{dw}{dr} \qquad (25)$$

$$\frac{d}{dr} \left\{ \mu\xi\theta + \frac{\gamma_* - 1}{2} M_*^2 w + v \right\} = 2C_* \frac{q\Lambda}{\sqrt{w}} \qquad (26)$$

$$p = \frac{\mu\theta}{r^2\sqrt{w}} \qquad (27)$$

$$\frac{dq}{dr} = \lambda_* \frac{q\Lambda}{r^2\sqrt{w}} \tag{28}$$

$$\frac{dE}{dr} = 2\lambda_* \left[\frac{L(EE_*)}{\Lambda_* E_*}\right] \frac{1}{r^2\sqrt{w}} \tag{29}$$

$$\alpha_d = \alpha_d(p,\theta) \tag{30}$$

$$\alpha_i = \alpha_i(p,\theta) \tag{31}$$

where

$$\mu = \frac{m_*}{m} = \frac{1 + C_a + 3C_i}{1 + C_a^* + 3C_i^*} \tag{32}$$

$$\xi = \left(\frac{\gamma}{\gamma-1}\right)\left(\frac{\gamma_*-1}{\gamma_*}\right) = \frac{7-2\alpha_d}{7-2\alpha_d^*} \tag{33}$$

$$\nu = \frac{\gamma_*-1}{\gamma_*} \frac{m_*}{m_H} \left[\frac{E_d}{2T_*} C_a + \frac{E_i}{T_*} C_i\right] \tag{34}$$

$$C_a = \frac{\alpha_d(1-\alpha_i)}{1-\alpha_i(1-\alpha_d)} \tag{35}$$

$$C_i = \frac{\alpha_d\alpha_i}{1-\alpha_i(1-\alpha_d)} \tag{36}$$

$$C_* = \left(\frac{\gamma_*-1}{\gamma_*}\right) \frac{2\pi r_*^2}{G} \frac{q_*}{T_*} m_* \lambda_* \tag{37}$$

$$\lambda_* = \frac{\rho_* \Lambda_* r_*}{2m_H} \tag{38}$$

In the above system of equations, M_* is the Mach number at r_*; w, θ, and ν are the normalized kinetic, thermal and potential energies of the flow. G is the mass ablation rate, and $m_H \lambda_*$ can be interpreted as the effective stopping mass of the ablatant.

Considering $\xi(\alpha_d)$, $\mu(\alpha_d,\alpha_i)$ and $\nu(\alpha_d,\alpha_i)$ as functions of p and θ, through lengthy algebraic manipulations, we can solve dw/dr and $d\theta/dr$ explictly [13]; thus

$$\frac{dw}{dr} = 4 \frac{C_* \psi_1(\theta,p) \tilde{M}^2 \frac{q\Lambda}{\sqrt{w}} - \frac{w}{r}}{1 - \tilde{M}^2 M_*^2 \psi_2(\theta,p)} \tag{39}$$

$$\frac{d\theta}{dr} = -4 \frac{C_* \psi_3(\theta,p) \frac{q\Lambda}{\sqrt{w}} - \psi_4(\theta,p) \frac{w}{r}}{1 - \tilde{M}^2 M_*^2 \psi_2(\theta,p)}, \tag{40}$$

where

$$\tilde{M}^2 = \frac{\gamma_*}{\gamma} \frac{w}{\mu\theta} = \frac{M^2}{M_*^2}, \tag{41}$$

and can be viewed as the normalized Mach number.

It is easy to demonstrate that in the limit of $\alpha_d \to 0$, Eqs. (39) and (40) reduce to the previous expressions of the TNS model. In summary, through the elimination of the mass density, ρ, we obtained five first-order nonlinear equations of p, w, θ, E and q. In Eqs. (39) and (40), we have four functional coefficients, ψ_1, ψ_2, ψ_3 and ψ_4, they involve μ, ξ, ν and their first derivatives with respect to p and θ. To determine these coefficients, we have to use the seven nonlinear algebraic equations describing α_d, α_i, μ, ξ, ν, C_a and C_i.

One observes that Eq. (39) and (40) become singular when $\tilde{M} = 1$, or Mach number of the flow $M(\equiv \tilde{M} M_*)$ becomes M_*, where

$$M_*^2 = 1/\psi_2(1,1) \ . \tag{42}$$

It follows then unless we are considering the special case of $\psi_2(T_*,p_*) = 1$, the singularity of Eqs. (39) and (40) do not necessary occur at the sonic radius. Since at $r = r_*$ (or $r' = 1$) all the normalized flow variables become unity, the definiteness of dw/dr then requires

$$C_* = 1/\psi_1(1,1) \ . \tag{43}$$

2.4. Initial conditions at the singular point

In view of the presence of the singularity of the governing equations, we shall analyze it as an initial value problem by specifying all the derivatives at the singular point. Thus, if we denote

$$\left.\frac{dw}{dr}\right|_{r=1} \equiv Z_s \ , \tag{44}$$

then [13]

$$\left.\frac{d\theta}{dr}\right|_{r=1} = \frac{4-A_w^* Z_s}{A_\theta^*} \ , \tag{45}$$

$$\left.\frac{dp}{dr}\right|_{r=1} = \frac{\gamma_* M_*^2 Z_s}{2} \ , \tag{46}$$

$$\left.\frac{dq}{dr}\right|_{r=1} = \lambda_* \ , \tag{47}$$

$$\left.\frac{dE}{dr}\right|_{r=1} = 2\lambda_* \frac{L(E_*)}{\Lambda_* E_*} \tag{48}$$

where parameters with asterisk are to be evaluated at the singular radius r = 1. The derivative Z_S is to be evaluated from Eq. (39) by applying L'Hôpital's rule. Formally, we may write Z_S as

$$Z_S = - Z_X \left(1 \pm \sqrt{1 - Z_Y}\right) . \tag{49}$$

where Z_X and Z_Y are complicated expressions involving the second derivatives of α_d and α_i with respect to p and θ. In the limit of $\alpha_d = \alpha_i = 0$, it can be shown that i.e. Z_S reduces to the previous expression of the TNS model, [13].

The above expression indicates that the specification of Z_S depends on the knowledge of the degree of dissociation, α_d^* and ionization, α_i^*, or equivalently p_* and T_* at r = 1. An examination of Eqs. (44)-(48) indicates that once p_* and T_* are given, there remain seven unknowns, ρ_*, v_*, E_*, q_*, r_*, G and λ_* to be specified. At the singular radius, $r = r_*$, there are five equations available

$$p_* = \rho_* T_* / m_* \tag{50}$$

$$\rho_* v_* r_*^2 = G/4\pi \tag{51}$$

$$M_*^2 = \frac{m_* v_*^2}{\gamma_* T_*} = \frac{1}{\psi_2(p_*, T_*)} \tag{52}$$

$$C_* = \frac{4\pi r_*^2}{G} \left(\frac{\gamma_* - 1}{2\gamma_*}\right) \frac{q_*}{T_*} m_* \lambda_* = \frac{1}{\psi_1(p_*, T_*)} \tag{53}$$

$$\lambda_* = \frac{\rho_* \Lambda_*(E_*) r_*}{2 m_H} \tag{54}$$

We recall that γ_* and m_* are functions of α_d^* and α_i^*, therefore, are determined once p_* and T_* are given. This leaves two parameters at our free disposal, E_* and λ_* (or alternatively E_* and G). This means once p_*, T_*, E_* and λ_* are specified, and the proper root of Z_S is chosen, all the five derivatives at $r = r_*$ are known.

2.5. Boundary conditions or compatibility requirement

The choice of the four parameters, p_*, T_*, λ_* and E_* cannot be arbitrary and must be compatible with the ablation process occurring at the pellet surface as well as with the ambient plasma state downstream at the cloud boundary.

a) Condition at the cloud boundary

At the cloud boundary, e.g. $r = r_b$, the energy and energy flux of the incoming electrons must correspond to their values of the ambient plasma. In terms of the normalized variables, these conditions can be written as the following:

$$\text{For } r \geq r_b \text{ , } E \to \tilde{E}(\equiv E_o/E_*) \text{ , and } q \to \tilde{q}(\equiv q_o/q_*) \tag{55}$$

where

$$\left.\begin{aligned} E_o &= 2T_e \\ q_o &= n_e \left(\frac{T_e}{2\pi m_e}\right)^{1/2} 2T_e \end{aligned}\right\} \tag{56}$$

b) Condition at the pellet surface

Owing to the lack of knowledge about the actual ablation process taking place at the pellet surface, we shall postulate two alternative possibilities and study their influence on the corresponding solutions obtained. These are the ideal energy absorption and dynamic phase transition.

i) The ideal energy absorbing process, [2]

In this case, we assume there exists a very effective energy absorbing layer within r_*, where most energy of the incoming electron is absorbed. By the time, the incoming electrons reaches the pellet surface, its energy flux q compared with q_* at r_* becomes vanishingly small, just sufficient to sublime the pellet material. As a result, the ablated vapor leaves the pellet with little thermal and kinetic energy. These conditions can be written formally as the following:

$$\left.\begin{aligned} &\text{At } r = \hat{r} \ (\equiv r_p/r_*) \ , \\ &\hat{q} \ (\equiv q_p/q_*) \to 0 \quad \text{and} \quad \hat{T} \ (\equiv T_v/T_*) \to 0 \ , \end{aligned}\right\} \qquad (57)$$

where T_v is the temperature of the ablated vapour near the pellet surface. For numerical analysis, we shall replace Eq. (57) by

$$\left.\begin{aligned} &\hat{q} < \hat{q}_c \ (\text{e.g. } \hat{q}_c = 1.0 \times 10^{-3}) \\ &\hat{T} < \hat{q} \ . \end{aligned}\right\} \qquad (57a)$$

ii) Dynamic phase transition, [14]

In this case, the energy flux, q_p is assumed to be sufficient to drive an evaporation front propagating towards the pellet in-

terior. The sufficient condition for this process to occur is given by [15],

$$\frac{\gamma}{2}\left(\frac{\gamma+1}{\gamma-1}\right) > \chi > \frac{\gamma}{\gamma-1} \tag{58}$$

where

$$\chi = \frac{q_p - q_s}{\phi_p T_v}$$

ϕ_p is the ablated particle flux,

$q_s = \phi_p \varepsilon$ is the energy flux required by the sublimation process, and $\varepsilon = 0.01$ eV is the sublimation energy per particle.

We like to remark here that the lower limit of χ differs from our previous result by a factor γ larger, [14]. This difference comes about because the previous limit is a necessary but not a sufficient condition [13]. When the ablatant leaves the pellet surface as a molecular gas, Eq. (58) becomes

$$4.2 > \chi > 3.5 \ . \tag{58a}$$

2.6. Method of solution

As mentioned previously, we shall solve the system of equations, Eqs. (25), (28), (29), (39) and (40), as an initial value problem. In other words, the integration is initiated by first evaluating their derivatives at $r = 1$.

Once the proper root of Z_s is chosen [13], we notice all the five derivatives at $r = 1$, Eqs. (44)-(48), are determined by the four parameters, T_*, p_*, E_* and λ_*. The four parameters are chosen in the following way: With T_e of the ambient plasma in mind, we first choose a value of E_*; T_* and p_* are then taken as a first guess from the previous solution of the TNS model, which cor-

responds to a frozen flow assumption. The integration is then initiated at $r = 1$ by selecting a value of λ_*, and continued inward numerically until the boundary condition at the pellet surface, Eq. (57a), or Eq. (58a), is satisfied. Once the pellet position is located, we then integrate outward until Eq. (55) is also satisfied to locate the cloud boundary.

For a given pellet radius, r_p and ambient plasma state of T_e and n_e, the proper solution must be obtained through a repeated iterative process. Compared with the single species TNS model, the iteration is more complicated. This is because if we even use the idealized energy absorption condition, Eq. (57), at the pellet surface, we have no freedom of choice for n_e and r_p once the four parameters, E_*, T_*, p_* and λ_* are chosen. In view of the temperature and density profiles present in the tokamak discharges, instead of carrying out the complicated iterative process for the solution of the ablation of a given pellet in a homogeneous plasma, we instead vary principally E_* (which corresponds mainly to the plasma temperature, T_e) in a suitable chosen range of interest. In case the solution yields unacceptable values of r_p and n_e, we then make a further adjustment of T_*, p_* and λ_* before repeating the integration process.

3. RESULTS

3.1. The effect of the ratio of the specific heats, γ

To study the possible influence of γ on the nature of the solution and ablation rate of the pellet, we have considered a specific example by taking $E_* = 20$ keV, $p_* = 1.4093 \times 10^7$ dynes/cm, and $T_* = 1.0$ eV at the singular radius, r_*. The eigenvalue λ is then chosen to satisfy the imposed boundary conditions of Eq. (57a) at the pellet surface and Eq. (55) at the ablated cloud boundary. The results obtained for the two approximations of γ corresponding to Eqs. (2a) and (2b) are shown in Table I.

Table I. Effect of the ratio of the specific heats.

γ	λ_*	$M_*^2 \times 10^{-1}$	r_*/r_p	r_p, cm	T_e, keV	$n_e \times 10^{12}$ cm^{-3}	G, kg/sec.
$\frac{7+3\alpha_d}{5+\alpha_d}$	0.8836	8.1996	1.497	3.179	11.2	3.588	4.744
$\frac{7-2\alpha_d}{5-2\alpha_d}$	0.8868	8.2002	1.491	3.204	11.2	3.577	4.779

From the tabulated results, one notices that neither the mass ablation rate, G, nor the plasma state, T_e, n_e and the pellet radius, r_p exhibit any marked difference in the two cases considered. In view of this finding, all the results mentioned hereafter refer only to the case where γ is taken as that given by Eq. (2a).

3.2. Influence of the ablation process at the pellet surface and the scaling law of the particle ablation rate

By taking the same ablated state of T_* and p_* at r_* as in the previous section, the solution of the system of governing equations corresponding to the two alternative ablation processes, Eqs. (57a) and (58a) were examined in the range of E_* from 1 to 20 keV. Comparing the results obtained, we notice that apart from a slight decrease of the eigenvalue λ_*, when condition (58a) is used, there is no significant difference either in the ablatant state or in the pellet radius and the ambient plasma state. For the two cases considered, the mass ablation rate, G, differs no more than 0.2 per cent. The scaling law of the ablation rate with respect to the pellet radius and the plasma state, as shown in Fig. 1, consequently is unaffected by the precise boundary condition at the pellet surface.

Explicitly, the particle ablation rate, $\dot{N}_p$, is given by [16]

$$\dot{N}_p = \left[\frac{4\pi}{(2\pi m_e)^{1/6}} \left(\frac{\gamma_* - 1}{m_H C_*^2}\right)^{1/3} M_*^{2/3}\right] \frac{\lambda_*}{(\hat{r}^4 \tilde{q} \hat{\lambda}_*^2)^{1/3}} (r_p^4 n_e)^{1/3} (T_e)^{1/2} \tag{59}$$

Comparing it with the ablation rate of the frozen flow, we see that both are essentially similar, except that $(\gamma-1)$ in the frozen flow expression is replaced by the factor $(\gamma_* - 1)\, M_*^2/C_*$, [16]. For values of p_* and T_* of interest, this factor is a nearly constant. The results shown in Fig. 1 can thus be written as

$$\dot{N}_p = (r_p^4 n_e)^{1/3}\, f(T_e) \tag{60}$$

For a H_2-pellet,

$$\left.\begin{aligned} f(T_e) &= 1.414 \times 10^{16}\, T_e^{1.439} \text{ when } 100 < T_e < 600 \text{ eV}, \\ &= 3.246 \times 10^{15}\, T_e^{1.673} \text{ when } 0.6 < T_e < 10 \text{ keV}. \end{aligned}\right\}$$

As a result of the dissociation and ionization of the ablatant, we observe that the ablation rate, as compared with that of the frozen flow, is reduced approximately by 15%.

3.3. Variation of the ablatant state in the cloud

The variation of the ablatant state with respect to the normalized expansion radius, r/r_p, is shown in Figs. 2 and 3 respectively, for the two cases considered. Figure 2 shows an example of a relatively high T_e, n_e and small r_p combination, representing a situation near the central region, whereas Fig. 3 shows that of a low T_e, n_e and large r_p combination representing the situation near the edge region of a tokamak discharge. The dotted curves in these figures give a comparison of the ablatant state based on the frozen flow approximation where effects of dissociation and ionization are neglected (TNS model).

One notices that the temperature variation exhibits the general feature of a phase transition process. The rise of the ablatant temperature during the expansion of the cloud is interrupted by two comparatively flat regions corresponding to the dissociation and ionization processes, respectively. This is accompanied by the drop of the flow velocity and the Mach number in the respective regions as shown in these figures. In contrast to these marked differences of the ablatant state from a frozen flow, no noticeable difference in the attenuation of the incoming electron energy or energy flux in the ablated cloud is detected.

3.4. Ionization radius and the validity of the spherical expansion

To simplify the analysis, in the model presented in Section 2, similar to the TNS model, we have assumed that the ablated cloud expands spherically from the pellet surface. A necessary requirement for the spherical expansion of the cloud is that the ablation of the pellet must proceed uniformly at the pellet surface. In a magnetized plasma, as the incoming electrons are guided by the magnetic field, uniform ablation cannot occur during the direct impact phase. However, once an extremely dense protective cloud is established through collisions with the ablated particles, the incident electrons become quickly randomized. In most cases of interest, one may expect that spherical expansion should be a reasonable approximation in the vicinity of the pellet where the electron-neutral collisional mean free path λ_{en} is much less than ρ_e, the local electron Larmor radius.

As the ablatant expands further downstream, its temperature rises and pressure drops; at some radius of expansion, its degree of ionization becomes appreciable. Consequently, the validity of spherical expansion once more should be examined. The degree of dissociation and of ionization of the ablatant depend on the local temperature and pressure within the ablated cloud. According to the method of solution used in the present analyses, they depend on their respective values, T_*, p_* or equivalently α_d^*

and α_i^*, imposed at r_*. By defining a dissociation radius, r_d where the concentration ratio $\rho H/\rho$ at the expansion radius, r_*, reaches a maximum and an ionization radius, r_i, where $\rho H^+/\rho = 0.995$, and taking some possible combinations of plasma state and pellet radius of interest, we have calculated values of r_d/r_p and r_i/r_p based on the present model; the results are given in Table II. From the results shown in the table, one notices that when α_d^* is held constant, the ratio r_d/r_p and r_i/r_p are nearly constant. They are neither sensitive to the variation of the plasma state of T_e and n_e nor to that of the pellet radius, r_p.

In the same table, we have also listed $(n_e)_{ri}$ and $(T_e)_{ri}$, the particle density and temperature of the ablated cold plasma at r_i. By equating the mean free path λ_e of the ablated cold electrons to the local electron Larmor radius, ρ_e, a critical field B_c can be introduced. Omitting the subscript r_i, B_c can be written explicitly as

$$B_c \text{ (gaus)} = 1.653 \times 10^{-13} (\ln\Lambda) n_e \text{ (cm}^{-3}) \; T_e^{-1.5} \text{ (eV)} \qquad (61)$$

where

$$\ln\Lambda = 23.1 + 1.5 \ln T_e - 0.5 \ln n_e, \; [20]. \qquad (61a)$$

Thus, for field strength $B < B_c$, the ablated cold plasma can be considered as "dense", spherical expansion of the ablated cloud can be taken as a reasonable approximation, [17].

Further information concerning the dissociation radius, r_d, ionization radius, r_i and the critical field, B_c for plasma state of fusion interest is given in Table III. One observes that due to the relatively high electron density of the ablatant at r_i, the critical field, B_c is rather high; at pellet radius, $r_p > 0.15$ mm, $B_c > 10$ Tesla. From the results shown in Tables II and III, we observe that a higher critical field is not necessary related to a larger ionization radius, the opposite seems to be the case.

In the region of the ablated cloud where ionization of the ablatant is in progress, the ablatant temperature is nearly a constant (e.g. Fig. 2), the magnitude of the critical field, B_c depends mainly on the electron density of the ablatant. The electron density of the ablatant depends both on the degree of ionization, α_i and the total particle density or the total mass density, ρ of the ablatant. For radius of expansion $r < r_i$, α_i increases, while ρ decreases rapidly with respect to the radius of expansion, one may, therefore, expect that the ablated electron density, and thus the critical field B_c attains a maximum somewhere in the intermediate region between r_d and r_i. An example illustrating this occurrence is given in Fig. 4.

In view of these observations, we like to remark here that the validity of the spherical expansion, in our opinion, should be examined in terms of B_c in conjunction with the attenuation of the energy flux of the incoming electrons, [18]. (The readers might noticed that for some identical values of plasma states and pellet radii, values of B_c reported in the present paper are lower than those given in reference [18], this discrepancy is due to the fact that instead of using the approximate value of $\ln\Lambda = 5$, a more accurate value of $\ln\Lambda$ according to Eq. (61a) was used in the present paper).

3.5. The possible occurrence of second singularity

The equation describing the kinetic energy of the ablatant, Eq. (39), becomes singular when

$$\tilde{M}^2 M_*^2 \phi_2 (\theta, p) = 1 . \qquad (62)$$

According to the definition of the normalized Mach number, $\tilde{M} = M/M_*$, this occurs when

$$\tilde{M}^2 = 1 , \quad \text{or } M_*^2 = 1/\phi_2(1,1) . \qquad (63)$$

This is the initial position, r_*, of our integration process. For some initial value of M_*, a second singularity can occur sometime further downstream of the flow, when the local Mach number, M becomes

$$M^2 = 1/\psi_2(\theta, p) \ . \tag{64}$$

In particular, this can take place when $\psi_2(\theta, p) = 1$ at some expansion radius, i.e. when the flow reverts to sonic. From the expression of $\psi_2(\theta, p)$, [13], it can be shown that $\psi_2(\theta, p) = 1$ at any one of the following situations:

$$\left.\begin{array}{ll} \text{i)} & \alpha_d = 0 \ , \text{ (i.e. the original TNS model)} \\ \text{ii)} & \alpha_d = 1 \ , \ \alpha_i = 0 \ , \\ \text{iii)} & \alpha_i = 1 \ . \end{array}\right\} \tag{65}$$

Owing to the presence of the Arrhenius factor in evaluating the equilibrium degree of dissociation, Eq. (10) $\alpha_d = 0$ cannot be attained in our present model. A close examination of the computational results, indeed, indicate that most breakdowns of the solution happen when $\psi_2(\theta, p) = 1$ and at the same time either $\alpha_d \approx 1$ (when $\alpha_d^* \approx 0$) or $\alpha_i \approx 1$ (when $\alpha_d^* \approx 1$). Examples of the occurrence of the second singularity under these circumstances are shown in Figs. 5 and 6. To check whether the occurrence of the second singularity is caused by computational round-off errors, we have perturbed the input parameters p_* and/or T_* slightly, and found that its occurrence persists. We have, therefore, suspected that this behaviour might be caused by a thermal shock, when a steep temperature gradient of the ablatant develops.

4. SUMMARY AND DISCUSSIONS

When a hydrogenic pellet of a given speed is injected into a fusion research device, e.g. tokamak, its penetration depth is determined mainly by its ablation rate in the prevailing plasma environment. The perturbation of the background plasma, such as the accompanying MHD activities, could be influenced to a great extent by the state of the ablatant, its temperature and its pressure, leaving the cloud. In view of these considerations, we have modified the transonic neutral shielding model (TNS model), [2], by considering the ablatant to be a mixture of four species; H_2, H, H^+, and electrons.

Based on the previous result of the TNS model that in the vicinity of the pellet the ablatant is extremely dense, we assumed that in a large portion of the ablated cloud, the LTE condition exists. The relative concentrations of these species, consequently, are determined by the local temperature and pressure in the cloud. In particular, we made no artificial separation of the dissociation and the ionization process.

To take into account the variation of the ratio of the specific heats, γ, due to dissociation, we used the argument that γ depends only on the degree of freedom, f, of the gas. Two possible variations of γ were then assumed: (i) f varies linearly with the degree of dissociation, α_d, and (ii) f is the average of the mixture of molecular and atomic hydrogen gas. Computational results indicated that there is no marked difference either in the pellet ablation rate or in the ablatant state when either one of the two alternatives is used (see Table I).

When a pellet is injected into a tokamak, or any other devices, it is subjected to the variation of the plasma temperature and density prevailing in the device. We have, therefore, investigated the ablation process extensively by taking various combinations of plasma state and pellet radius of practical in-

terest into consideration, and derived a scaling law. Results of the analyses (Fig. 1) showed that the pellet ablation rate scales in the same way with respect to the ambient plasma state and the pellet radius as that of a frozen flow (the TNS model). The presence of dissociation effect reduced the ablation rate by approximately 15%.

When dissociation and ionization effects are present, the temperature and velocity profile of the ablatant showed the typical behaviour of a phase transition phenomenon; it is distinctively different from those of a frozen flow. On the other hand, there is no noticeable difference in the attenuation of the incoming electron energy or energy flux in the cloud whether the ablatant is in a frozen or in an equilibrium state (see Figs. 2 and 3).

In view of the uncertainty of the evaporation process at the pellet surface, we have used two alternative boundary conditions: (i) the zero energy flux approximation [2], and (ii) the dynamic phase transition [14]. Results of the analyses revealed that neither the pellet ablation rate nor the state of the ablatant showed a marked difference with respect to the two alternatives used. A possible explanation concerning this finding might be due to the fact that as long as the state of the ablatant and the energy flux of the incoming electrons are the same at the singular radius, the stopping property of the ablatant is nearly the same.

To simplify the analyses, similar to the TNS model, [2], we have assumed the ablatant expands spherically. This approximation requires a close examination once the ablatant is sufficiently ionized. Previous results based on the TNS model showed that most of the incoming electron energy is absorbed in a relatively thin layer around the pellet. We, therefore, studied the possible existence in the present model of such a spherical shell. It was shown that the presence of such an effective energy absorbing layer could be based on the comparison between the local ablated electron collisional mean free path with the electron Larmor radius in the cloud. Based on this, a critical field, B_c, was

introduced. An effective energy absorbing spherical shell exists when the local field strength $B < B_c$. By defining an ionization radius, r_i, where 99.5% of the ablated material is ionized; B_c was evaluated at r_i. Results of the analyses then showed that a large r_i does not necessary correspond to a high B_c. For most combinations of plasma states and pellet radii; in fact, the opposite seems to be the case (see Tables II and III). At plasma state of fusion interest and pellet radius exceeds 0.15 mm, the critical field, B_c at r_i is well beyond 10 Tesla (see Table III).

Due to the presence of the singularities, we solved the system of governing equations as an initial value problem by a proper choice of the four parameters, p_*, T_*, E_* and λ_* at the singular radius of expansion, r_*. For a given plasma state and pellet radius combination, the problem has to be solved through a complicated iteration process. We have circumvented this difficulty by varying the plasma state and pellet radius over a wide range of interest, and derived a scaling law of the pellet ablation rate. On the other hand, we are still prevented from formulating a scaling law concerning the state of the ablatant with respect to a given combination of plasma state and pellet radius. The task is made more difficult because for some combinations of ambient plasma state and pellet radius, a second singularity sometimes appears further downstream from r_*, where the ablated fluid reverts to a subsonic flow. This phenomenon, as mentioned previously in Section 3.5, apparently is not caused by computational round-off errors, but might have some real physical implications. In this respect, it is of interest to note that in a somewhat related problem in comet researches, the possible occurrence of an inner shock has been suggested [19].

The main idea of the TNS model as well as the present one is to consider the ablatant as an effective stopping medium of the incoming plasma electrons. To simplify the analysis, we have taken both the loss function, $L(E)$, and the effective attenuation cross section of the energy flux, $\Lambda(E)$, of the ablated mixture to be identical to those of a molecular hydrogen gas. This approximation seems to be reasonable as long as the ablatant remains

only weakly ionized. In view of the possible excitation of plasma waves through the interaction of the hot incoming electrons with a relatively cold ablated plasma [21], the validity of this approximation, and its possible consequence on the pellet ablation rate of a moderately or fully ionized ablatant remains a subject requiring further study.

APPENDIX

Derivation of the expressions, $\frac{dq}{dr}$, $\frac{dE}{dr}$ and $\Lambda(E)$

Denoting different types of the target particles (i.e. the different species of the ablatant) by the subscript "j", the attenuation of the energy flux of the incoming electrons in the ablatant can be written as

$$\frac{dq}{dr} = q\Sigma_j n_j \Lambda_j(E) \qquad (A-1)$$

$$= q\{n_H \Lambda_{H_2}(E) + n_H \Lambda_H(E) + n_{H^+} \Lambda_{H^+}(E) + n_e \Lambda_e(E)\}$$

Assuming that back scattering of the incoming electrons mainly is due to the impact with the nuclei of the target particles, we can then put

$$\sigma_{H^+}(E) = \sigma_H(E) = \sigma_{H_2}(E)/2 \ . \qquad (A-2)$$

Using Block's rule, we have

$$L_H(E) = \frac{1}{2} L_{H_2}(E) \ . \qquad (A-3)$$

As a result,

$$\Lambda_H(E) = \frac{\sigma_{H_2}(E)}{2} + \frac{2L_{H_2}(E)}{2E} = \frac{\Lambda(E)}{2} \qquad (A-4)$$

where

$$\Lambda(E) \equiv \sigma_{H_2}(E) + 2\,\frac{L_{H_2}(E)}{E} \equiv \Lambda_{H_2}(E) \qquad \text{(A-5)}$$

The attenuation of the energy flux of the incoming electrons due to interaction with the cold plasma of the ablatant is represented by

$$n_{H^+}\Lambda_{H^+}(E) + n_e\Lambda_e(E) = n_{H^+}\left\{\sigma_{H^+}(E) + \sigma_e(E) + 2\,\frac{L_{H^+}(E)}{E} + 2\,\frac{L_e(E)}{E}\right\}$$

$$\approx n_{H^+}\left\{\sigma_{H^+}(E) + 2\,\frac{L_e(E)}{E}\right\} \qquad \text{(A-6)}$$

In the above approximation, we have neglected $L_{H^+}(E)$ compared with $L_e(E)$ and $\sigma_e(E)$ compared with $\sigma_{H^+}(E)$. Taking into account that the energy loss of electron impact to a free electron is nearly the same as that to a bound electron, we may write

$$L_e(E) \approx L_H(E)$$

(see the following remark concerning this approximation). Replacing $\sigma_{H^+}(E)$ by $\sigma_H(E)$, Eq. (A-6) finally reduces to

$$n_{H^+}\Lambda_{H^+}(E) + n_e\Lambda_e(E) \approx \frac{n_{H^+}}{2}\,\Lambda(E)\ . \qquad \text{(A-6a)}$$

Substituting Eq. (A-4) and (A-6a) into Eq. (A-1), we have

$$\frac{dq}{dr} \approx q\,\frac{\Lambda(E)}{2}\left\{2n_{H_2} + n_H + n_{H^+}\right\}\ .$$

In terms of the mass density, ρ, of the mixture, finally, we obtain

$$\frac{dq}{dr} = \frac{\rho q \Lambda(E)}{2m_H} .$$

Using the same approximation, it is easy to show that

$$\frac{dE}{dr} = \frac{\rho}{m_H} L(E)$$

Recalling that $m_{H_2} = 2m_H$, these expressions formally have the same appearance as those of the TNS model.

Remark concerning the approximation of $L_e(E) \simeq L_H(E)$

When the energy, E, of the incident electrons is much greater than the thermal energy T_{cp} of the cold electrons of the ablatant, the attenuation of the incident electron energy due to collisions with cold plasma ions can be neglected. Using the Coulomb collisional theory [20], and taking the Coulomb logarithm, $L_C \simeq 10$, we calculated the loss function $L_e(E)$ in the range of incident electron energy, $20 < E < 2 \times 10^4$ eV for two values of T_{cp}, 25 and 50 eV. The result is shown in Fig. 6. It is to be noted that except for a shift of the maximum towards a higher E, $L_e(E)$ is insensitive to T_{cp} when $E > 1$ keV.

For $E >> T_{cp}$, due to the collective effect, plasma waves can be excited (Cherenkov radiation) in the cold plasma; this effect is neglected in the usual binary collisional approach. To check this possible additional loss, we resorted to the asymptotic expression given by Kihara and Aono, [21]. In terms of the loss function, denoted here by $L_{cp}(E)$, their expression can be written as

$$L_{cp}(E) = \frac{2\pi e^4}{E} \ln\left(\frac{mv^3}{e^2\omega_p}\right) \qquad (A-7)$$

where $v = (2E/m_e)^{1/2}$ is the incident electron velocity, and $\omega_p = (4\pi e^2 n/m_e)^{1/2}$ is the plasma frequency. For comparison, $L_{cp}(E)$ is also shown in Fig. 7 for incident electron energy

$E > 1$ keV at two values of the cold plasma density, $n_{cp} = 10^{16}$ and 10^{18} cm^{-3}. Comparing these results with those of the semi-empirical formula, $L_H(E)$, and the loss function, $L_e(E)$, we observe that at $E > 3$ keV, they all have the nearly same $1/E$ dependence. At high values of E, the presence of the collective effect can increase the loss function by a factor of around 2. The results shown in the figure also indicated that at a low incident electron energy ($E < 1$ keV), the approximation of $L_e(E)$ by $L_H(E)$ might lead to an underestimate.

Table II. Ionization radius, r_i and the critical field, B_c, $p_* = 2.197 \times 10^7$ dynes/cm^2

T_* eV	E_* keV	λ_*	r_p mm	T_e keV	n_e 10^{13}cm^{-3}	r_d/r_p	r_i/r_p	$(n_e)r_i$ 10^{16}cm^{-3}	$(T_e)r_i$ eV	B_c tesla
0.9	2.5	0.5557	0.269	1.40	13.5	1.57	21	2.95	1.89	0.93
($\alpha_d^* = 0.998528$)	5.0	0.5467	0.850	2.76	4.93	1.56	21.3	3.02	"	0.96
	6.5	0.5419	1.31	3.57	3.38	1.58	21.4	3.10	"	0.98
	7.5	0.5391	1.66	4.11	2.75	1.62	21.5	3.12	"	0.98
	7.8	0.5383	1.80	4.27	2.60	1.63	21.5	3.12	"	0.98
1.0	7.0	0.8118	2.99	3.99	2.60	1.32	12.8	5.74	2.06	1.59
($\alpha_d^* = 0.999221$)	7.5	0.8109	3.36	4.27	2.36	1.28	12.7	5.8	"	1.64
	7.8	0.8098	3.59	4.43	2.23	1.30	12.7	5.78	"	1.62
1.05	7.8	0.9518	4.70	4.51	2.16	1.26	10.1	8.02	2.14	2.10
1.0643	7.3	0.9941	4.51	4.26	2.37	1.20	9.59	8.79	2.13	2.34

Table III. Ionization radius, r_i and the critical field, B_c for plasma state of fusion interest

a) $E_* = 20$ keV

T_* eV	p_* 10^9 dynes/cm^2	λ_*	r_p mm	T_e keV	n_e 10^{14}cm^{-3}	r_*/r_p	r_d/r_p	r_i/r_p	$(n_e)r_i$ 10^{18}cm^{-3}	$(T_e)r_i$ eV	B_c tesla
1.2	1.5	0.5231	0.159	10.77	5.04	1.96	1.92	25.2	1.33	3.24	15
1.6	1.5	0.9657	0.540	11.34	4.40	1.48	1.27	10	3.81	3.97	32
1.8	1.5	1.1130	0.753	11.52	4.65	1.43	1.20	7.40	6.0	4.32	44
1.8	1.0	1.1760	1.23	11.59	3.15	1.41	1.17	6.36	5.44	4.23	41
1.8	0.5	1.2660	2.79	11.70	1.65	1.39	1.12	5.02	4.48	4.28	31

REFERENCES

[1] SCHMIDT, G.L., MILORA, S.L., ARUNASALAM, V. et al., in plasma physics and Controlled Nuclear Fusion Research 1986 (Proc. 11th Int. Conf. Kyoto, 1986), Vol. 1 IAEA, Vienna (1987) 171; GREENWALD, M., BESEN, M., CAMACHO, F., et al., ibid, 139; NIEDERMEYER, H., WAGNER, F., BECKER, G., et al., ibid, 125.

[2] PARKS, P.B., TURNBULL, R.J., Phys. Fluids 21 (1978) 1735.

[3] MILORA, S.L., FOSTER, C.A., IEEE Transactions on Plasma Science, PS-6 (1978) 578.

[4] KAUFMANN, M., LACKNER, K., LENGYEL, L., SCHNEIDER, W., Nucl. Fusion 26 (1986) 171.

[5] WATKINS, M.L., HOULBERG, W.A., CHEETHAM, A.D., et al., in Controlled Fusion and Plasma Physics (Proc. 14th Eur. Conf. Madrid, 1987), Vol. 11D, Part I, European Physical Society (1987) 201.

[6] PARKS, P.B., Nucl. Fusion 20 (1980) 311.

[7] THOMAS, C.E., An Experimental Investigation of Solid Hydrogen Pellet Ablation in High Temperature Plasma Using Holographic Interferometry and Other Diagnostics, Rep. ORNL/TM-7486, Oak Ridge National Lab. (1981).

[8] MILORA, S.L., Journal of Fusion Energy 1 (1981) 15.

[9] TFR Group, Europhys. Lett. 2 (1986) 267.

[10] BÜCHL, K., VLASES G.C., SANDMANN, W., LANG, R., Nucl. Fusion 27 (1987) 1939.

[11] PARKS, P.B., Model of an Ablating Solid Hydrogen Pellet in a Plasma, Ph.D. Thesis, Univ. of Illinois, Urbana-Champain, 1977.

[12] FELBER, F.S., MILLER, P.H., PARKS, P.B., et al., Nucl. Fusion 19 (1979) 1061.

[13] CHANG, C.T., THOMSEN, K., PIRET, S., Effect of Ablatant Composition on the Ablation of a Fuelling Pellet, Rep. Risø-M-2678, Risø National Laboratory, Roskilde, Denmark (1988).

[14] CHANG, C.T., Phys. Fluids 26 (1983) 805.

[15] CHANG, C.T., Some Open Questions Concerning the Neutral-Shielding Model of a Fuelling Pellet, Rep. Risø-M-2563, Risø National Laboratory, Roskilde, Denmark (1986).

[16] CHANG, C.T., THOMSEN, K., in Controlled Fusion and Plasma Physics (Proc. 12th Europ. Conf. Budapest, 1985), Vol. 9F, Part II, European Physical Society (1985) 656.

[17] ALFVÉN, H., FÄLTHAMMAR, C.G., Cosmical Electrodynamics, 2nd Ed. Oxford Univ. Press, Oxford (1963) 161.

[18] CHANG, C.T., On the Effective Spherical Energy Absorbing Region of the Neutral Shielding Pellet Ablation Model, submitted to Nucl. Fusion.

[19] IP, W.-H. in Advances in Space Plasma Physics (Buti, B. Ed.), World Scientific, Singapore (1985) 4.

[20] SIVUKIN, D.V., in Review of Plasma Physics, Vol. 4 (Leontovich, M.A., Ed.), Consultants Bureau, New York (1966) 93.

[21] SCHUNK, R.W., HAYES, P.B., Planet. Space Sci. 19 (1971) 113.

FIGURES

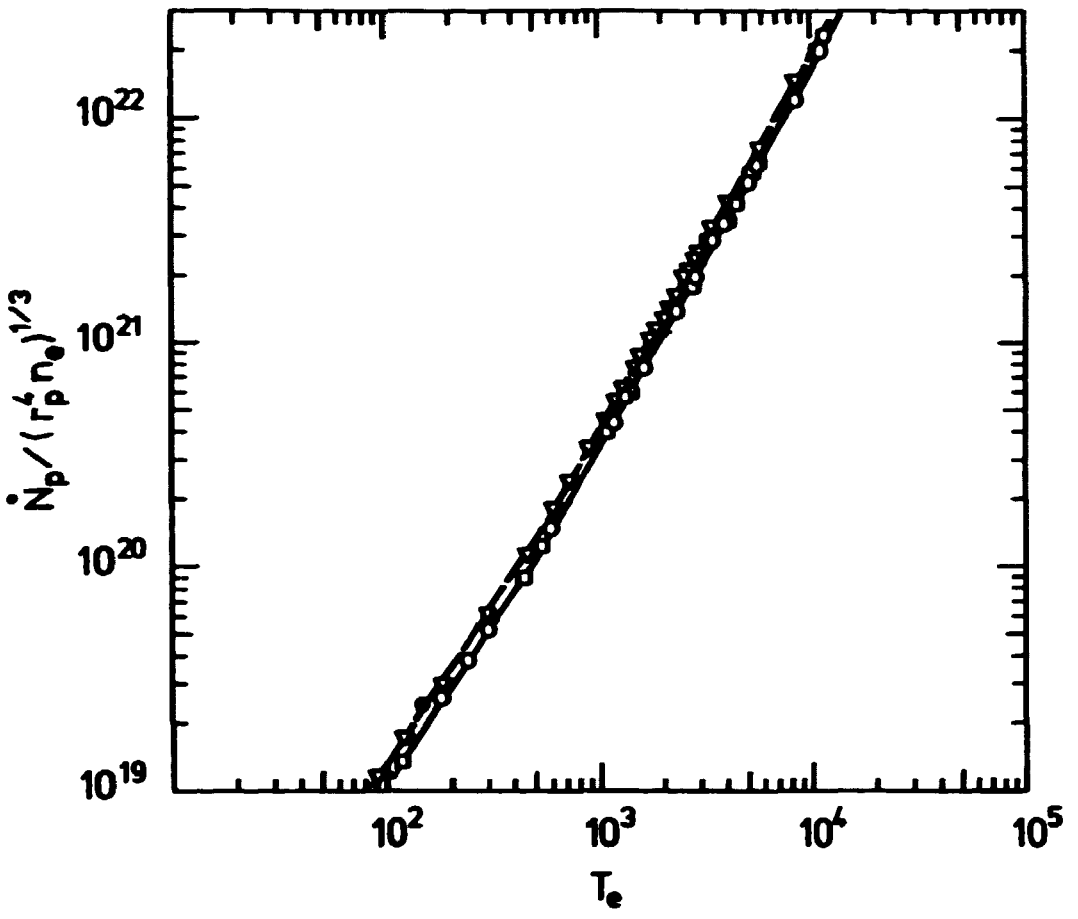

Fig. 1. Variation of $\dot{N}_p/(r_p^4 n_e)^{1/3}$ vs. plasma electron temperature, T_e. The dashed curve corresponds to a frozen, the solid one an equilibrium ablated flow. Boundary conditions $\hat{q} > \hat{T}$, $\hat{q} < 1.0 \times 10^{-3}$ or $4.2 > x > 3.5$, and Eq. (55).
Legend: 0, fixed degree of dissociation at the singular radius, $\alpha_d^* = 0.9995$. □ α_d^* varied. •, result of the equilibrium flow where a second singularity is present.

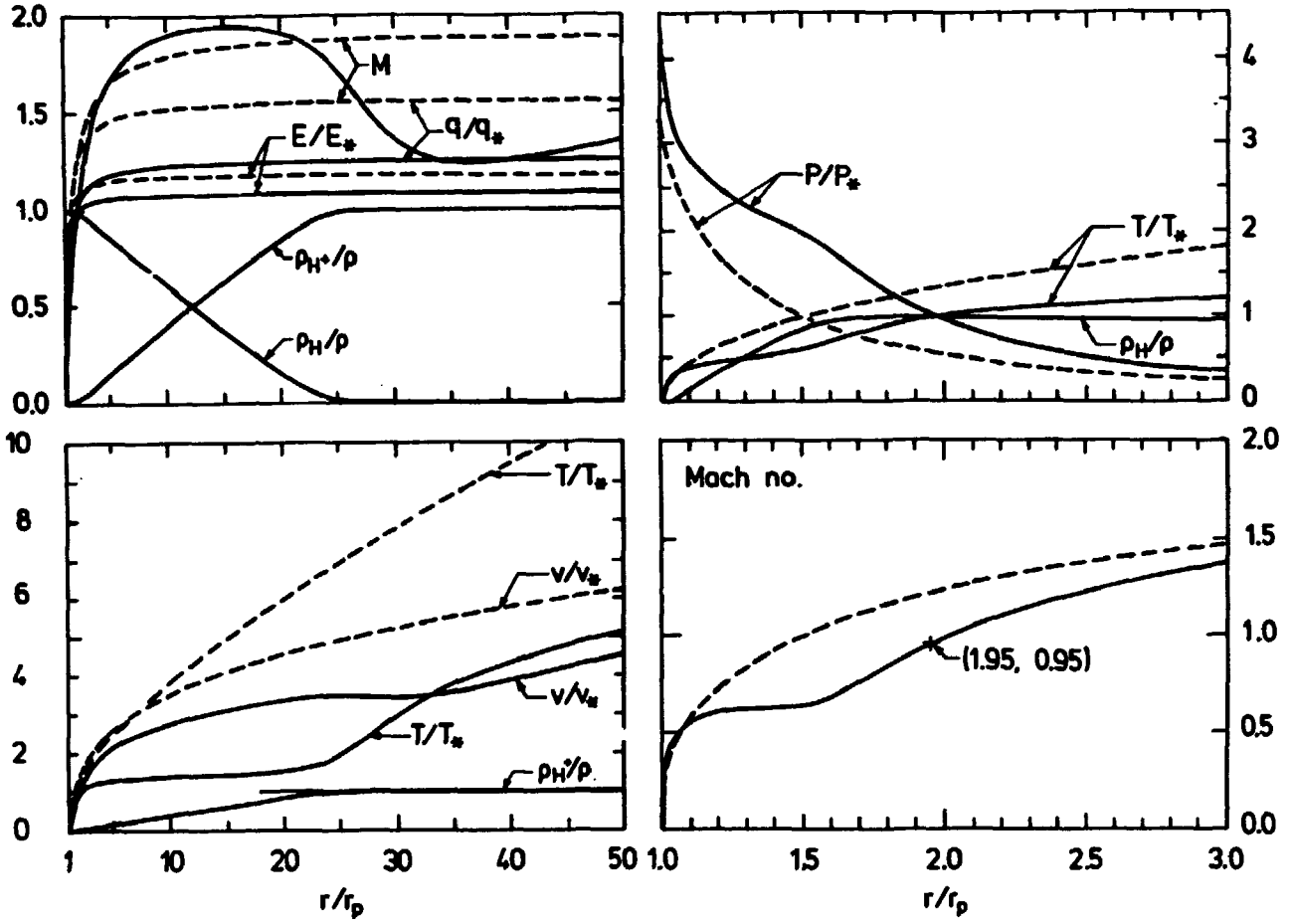

Fig. 2. Variation of the ablatant state with the normalized expansion radius, r/r_p. Plasma state and the pellet radius: T_e = 2.73 keV, n_e = 9.93 × 10^{13} cm, r_p = 0.36 mm. The dashed curves represent the corresponding state of a single-species fluid. The normalization parameters for the 4-species and 1-species ablatant are respectively: q_*, 6.0 × 10^7 (4), 4.88 × 10^7 (1) w/cm^2; E_*, 5.0 (4), 4.63 (1) keV; T_*, 0.9 (4), 1.35 (1) eV; V_*, 1.14 × 10^6 (4), 0.95 × 10^6 (1) cm/s; p_*, 4.0 × 10^7 (4), 7.2 × 10^7 (1) dynes/cm^2. The singular radius of expansion are respectively r_*/r_p, 1.95 (4), 1.5 (1).

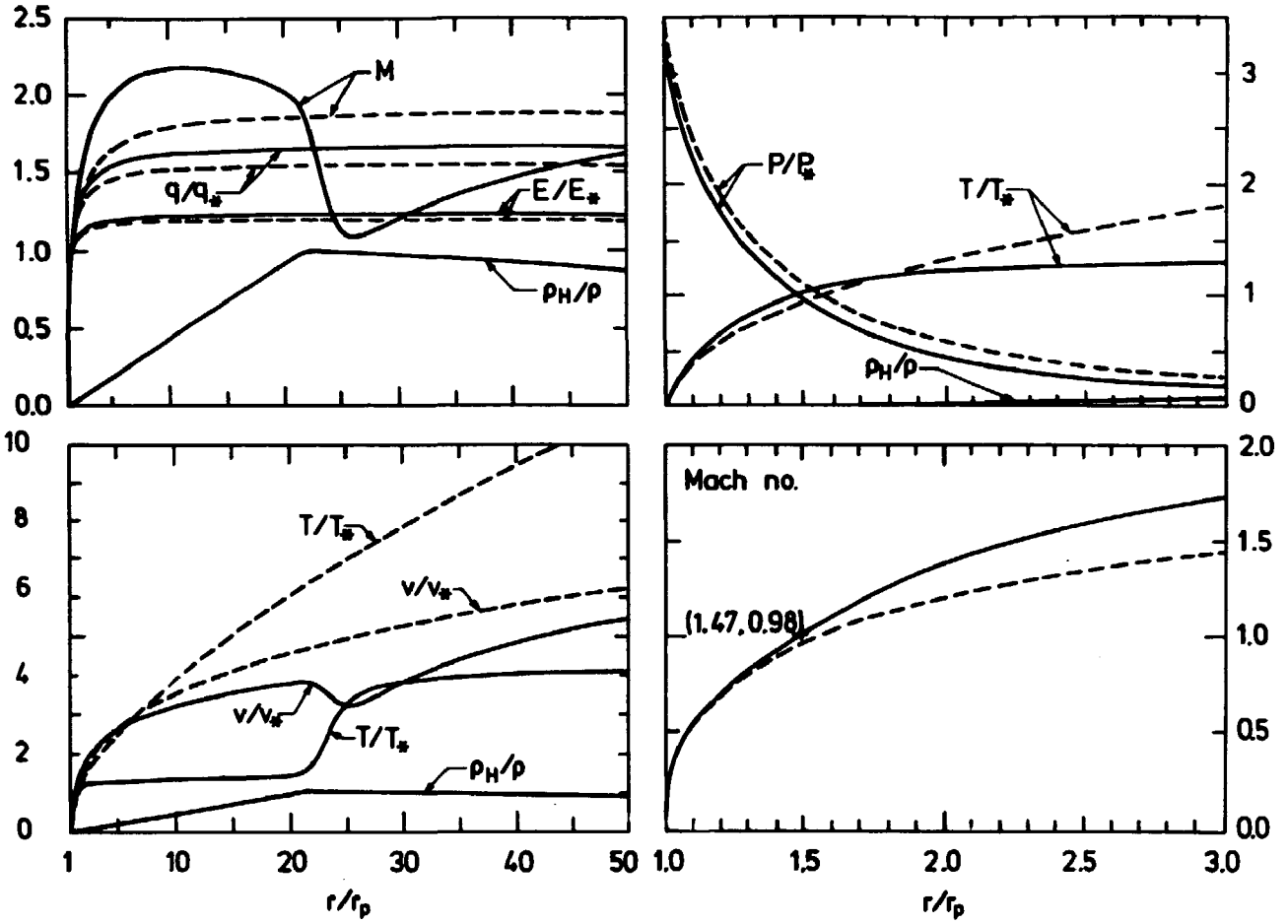

Fig. 3. Variation of the ablatant state with the normalized expansion radius, r/r_p. Plasma state and the pellet radius: T_e = 124 eV, $n_e = 7.15 \times 10^{11}$ cm^{-3}, r_p = 1.66 mm. The dashed curves represent the corresponding ablatant state of a single-species fluid. The normalization parameters for the 4-species and 1-species ablatant are respectively: q_*, 3.17×10^3 (4), 3.41×10^3 (1) w/cm^2; E_*, 200 (4), 206 (1) eV; T_*, 0.15 (4), 3.64 (1), eV; V_*, 0.31×10^6 (4), 1.56×10^6 (1) cm/s; p_*, 1.5×10^4 (4), 0.30×10^4 (1) dynes/cm^2. The singular radius of expansion are respectively r_*/r_p, 1.47 (4), 1.56 (1).

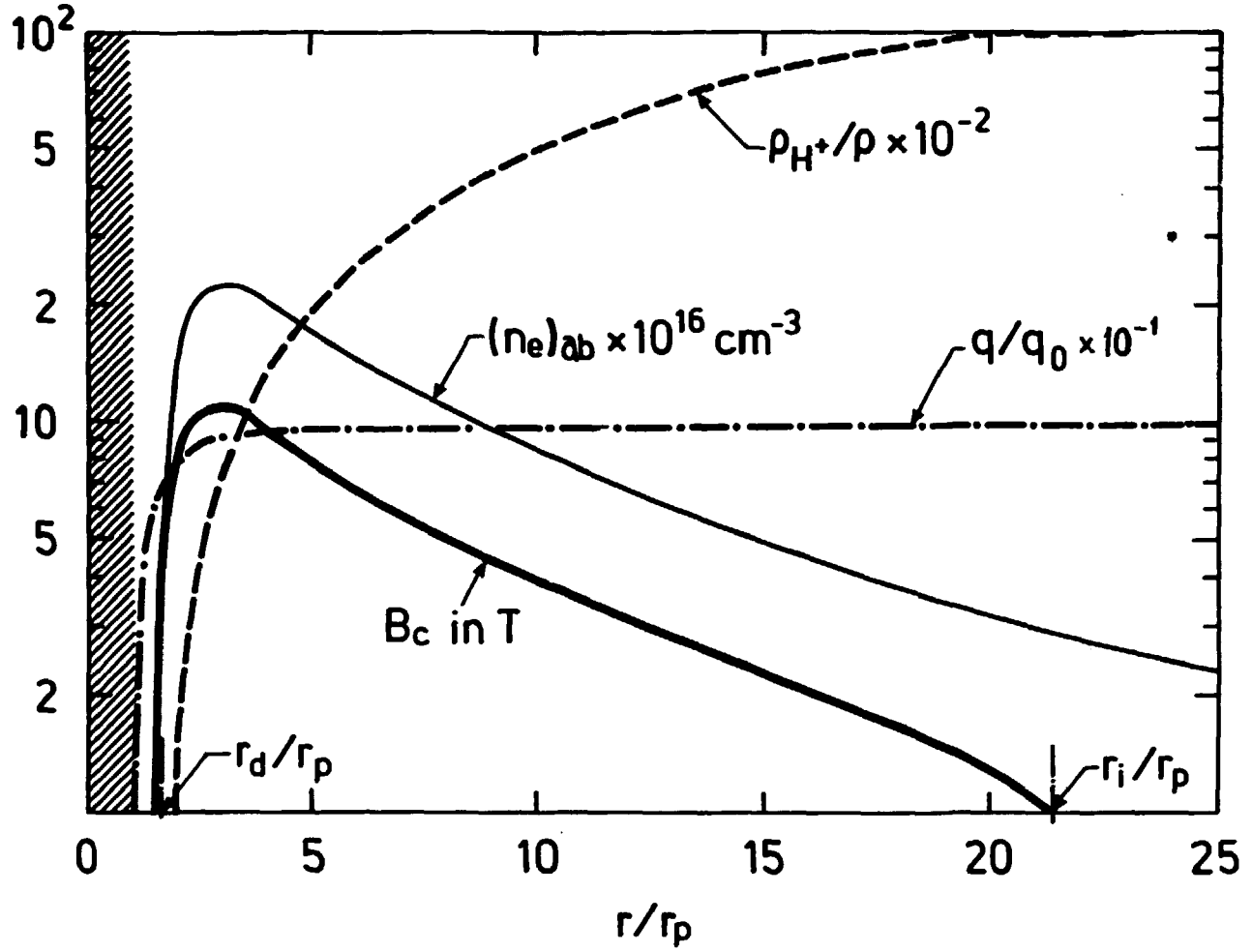

Fig. 4. Variation of the critical field, B_c, ablated electron density, $(n_e)_{ab}$, concentration ratio, $\rho_H{}^+/\rho$, and the energy flux ratio, q/q_0 with the normalized expansion radius, r/r_p. Plasma state and pellet radius: T_e = 3.57 keV, $n_e = 3.38 \times 10^{13}\ cm^{-3}$, r_p = 1.31 mm.

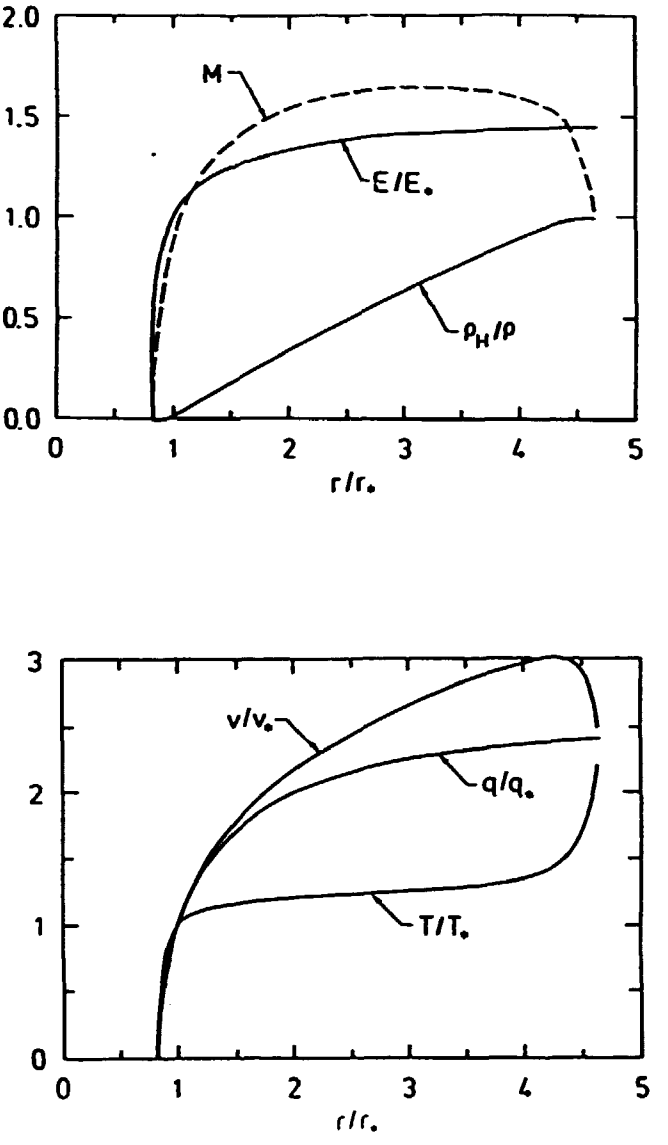

Fig. 5. Example illustrates the occurrence of a second singularity where $\alpha_d = 1.$ $\alpha_d^* = 0.02$ at the first singular radius, r_*. Plasma state and pellet radius: $T_e = 145$ eV, $n_e = 2.54 \times 10^{12}$ cm^{-3}, $r_p = 1.32$ mm.

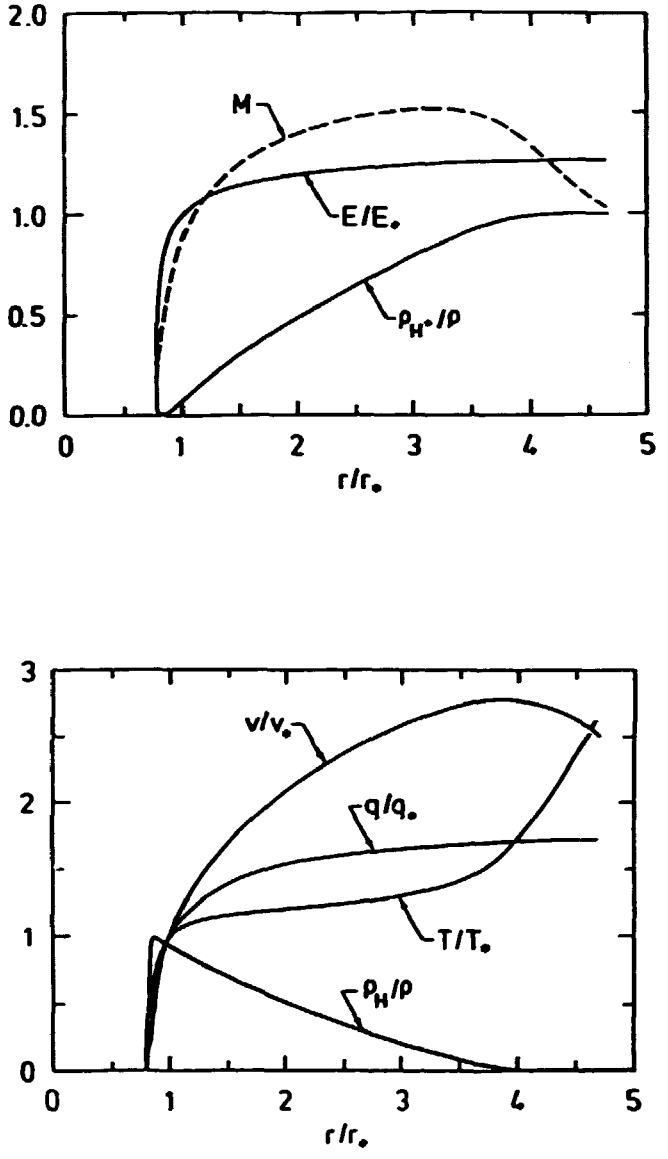

Fig. 6. Example illustrates the occurrence of a second singularity where $\alpha_i = 1$. $\alpha_d^* = 0.9999$ at the first singular radius, r_*. Plasma state and pellet radius: $T_e = 636$ eV, $n_e = 1.54 \times 10^{14}$ cm^{-3}, $r_p = 1.11$ mm.

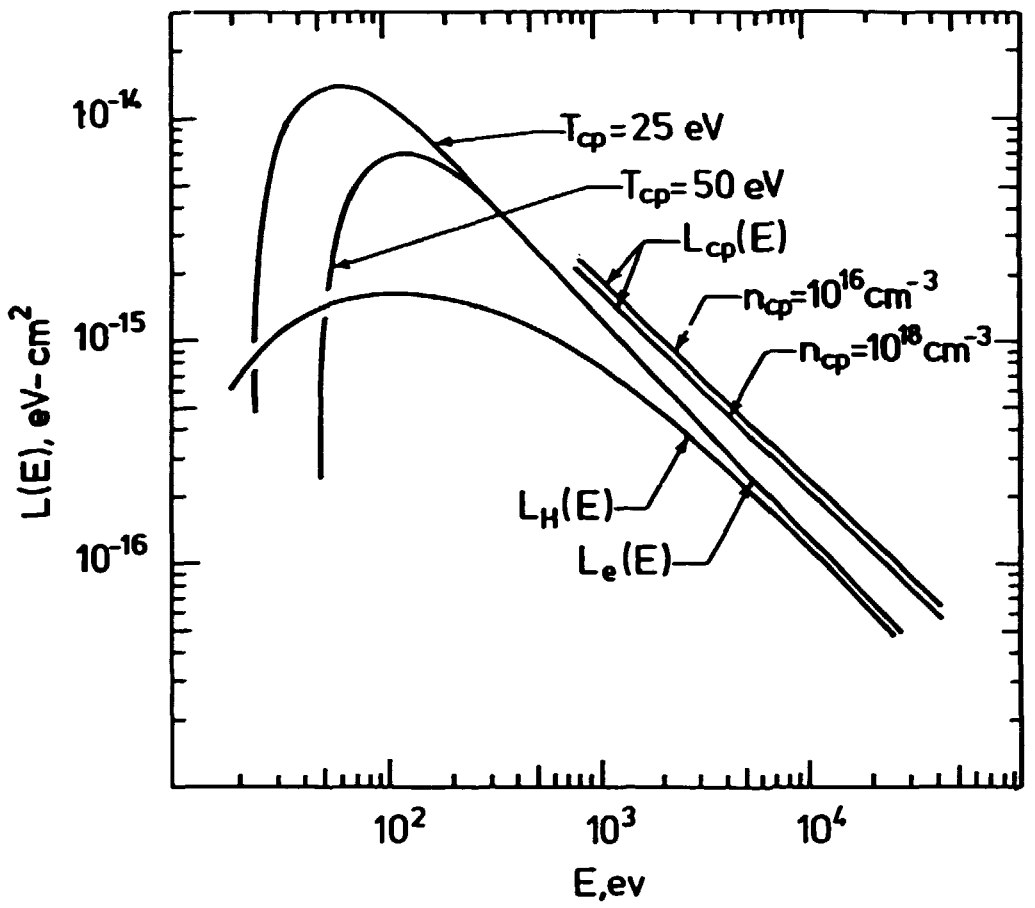

Fig. 7. Loss function L(E) vs. incident electron energy, E. $L_H(E)$ is the loss function of electrons in the atomic hydrogen gas, where $2L_H(E) = L_{H_2}(E)$ of Eq. (20). $L_e(E)$ is the loss function in the plasma based on Coulomb collisions. $L_{cp}(E)$ shows the effect of "Cherenkov radiation" for additional energy loss of hot electrons in a cold target plasma.

Risø National Laboratory **Risø - M - 2748**

A MODEL OF PELLET ABLATION WITH A MULTI-SPECIES ABLATANT

C.T. Chang and K. Thomsen
Risø National Laboratory - Association Euratom

S. Piret
Laboratoire de Physique des Gaz et des Plasmas
Université Paris-sud, Orsay, France

Date October 1988

Department or group
Physics Department

Groups own registration number(s)

Project/contract no.

Pages 50 Tables 3 Illustrations 7 References 21

ISBN 87-550-1466-6

Abstract (Max. 2000 char.)

The single species neutral - shielding model for the ablation of a hydrogenic pellet is extended by considering the ablatant as a mixture of four species: molecular and atomic hydrogen, protons and electrons. Compared with the single - species - ablatant model, results of the analysis showed that the ablatant state differs considerably. The attenuation of the incoming electron energy and energy flux, however, are very much similar, irrespective of the ablatant composition. The scaling law of the pellet ablation rate with respect to the plasma state of T_e, n_e and the pellet radius, r_p remains the same; the ablation rate is reduced approximately by 15%. At some combinations of T_e, n_e and r_p, a weak shock can appear when the ablated flow downstream becomes sonic. A sufficient but not necessary condition for its occurence is that the ablatant approaches either a state of complete dissociation, or complete ionization. To study the possible existence of an effective energy absorbing spherical region around the pellet, a comparison between the local ablated electron collisional mean free path and the electron Larmor

(Continued next page)

Descriptors

Available on request from Risø Library, Risø National Laboratory, (Risø Bibliotek, Forskningscenter Risø),
P.O. Box 49, DK-4000 Roskilde, Denmark.
Telephone 02 37 12 12, ext. 2262. Telex: 43116, Telefax: 02 36 06 09

radius in the cloud is made. A critical field, B_c is then defined and evalued at the ionization radius, r_i. For plasma state of fusion interest and pellet radius beyond 0.15 mm, B_c is well above 10 Tesla.

Available on exchange from:
Risø Library,
Risø National Laboratory,
P.O. Box 49, DK-4000 Roskilde, Denmark
Phone (02) 37 12 12 ext. 2262

ISBN 87-550-1466-6
ISSN 0418-6435